

Ground-state properties of Ca_2 from narrow line two-color photoassociation

Evgenij Pachomow,¹ Veit Peter Dahlke,¹ Eberhard Tiemann,² Fritz Riehle,¹ and Uwe Stern¹

¹Physikalisch-Technische Bundesanstalt (PTB), Bundesallee 100, 38116 Braunschweig, Germany

²Institut für Quantenoptik, Leibniz Universität Hannover, Welfengarten 1, 30167 Hannover, Germany

(Dated: December 3, 2024)

By two-color photoassociation of ${}^{40}\text{Ca}$ four weakly bound vibrational levels in the $\text{Ca}_2 \text{X}^1\Sigma_g^+$ ground state potential were measured, using highly spin-forbidden transitions to intermediate states of the coupled system ${}^3\Pi_u$ and ${}^3\Sigma_u^+$ near the ${}^3P_1 + {}^1S_0$ asymptote. From the observed binding energies, including the least bound state, the long range dispersion coefficients C_6, C_8, C_{10} and a precise value for the s-wave scattering length of $308.5(50) a_0$ were derived. From mass scaling we also calculated the corresponding scattering length for other natural isotopes. From the Autler-Townes splitting of the spectra, the molecular Rabi frequency has been determined as function of the laser intensity for one bound-bound transition. The observed value for the Rabi-frequency is in good agreement with calculated transition moments based on the derived potentials, assuming a dipole moment being independent of internuclear separation for the atomic pair model.

PACS numbers: 34.50.Rk, 34.20.Cf, 33.15.Kr

I. INTRODUCTION

Photoassociation (PA) of ultracold atoms is a valuable tool to accurately determine interatomic interactions, to create ultracold molecules [1], or to modify their scattering properties by optical Feshbach resonances [2]. In the PA process two atoms collide in the presence of a light field, inducing transitions from the atom-atom scattering continuum to bound molecular states at relatively large internuclear distances R . Therefore, the PA process is sensitive to the long range parts of the interaction potentials. Two-color PA via an excited molecular state to states in the ground molecular potential allows probing the interaction of two atoms in their electronic ground states. It has been used with great success for the investigation of binding energies and scattering lengths of alkaline atoms Li [3], Na [4], K [5], Rb [6], Cs [7], and more recently for systems with two valence electrons He* [8], Sr [9] and Yb [10].

In this paper we report on the first two-color PA of the alkaline-earth isotope ${}^{40}\text{Ca}$. It has an electronic structure similar to Sr and Yb but for the atomic intercombination line a much narrower width of 374 Hz [11] compared to 7 kHz in Sr or 182 kHz in Yb. Due to its relatively simple electronic structure calcium is a good model system to investigate the theoretical predictions for lineshape and rate of collisions in the presence of laser fields given by the model of Bohn and Julienne [12, 13]. We have measured the four least bound states ($v = 40, J = 0$; $v = 39, J = 0, 2$; $v = 38, J = 2$) in the ${}^{40}\text{Ca}_2 \text{X}^1\Sigma_g^+$ ground state potential using strongly spin-forbidden intercombination transitions to intermediate states near the ${}^1S_0 + {}^3P_1$ asymptote (Fig. 1).

Our measurements complement the short range ground-state potential determined by molecular spectroscopy [14] that provided information about the interaction potential up to 2 nm internuclear separations.

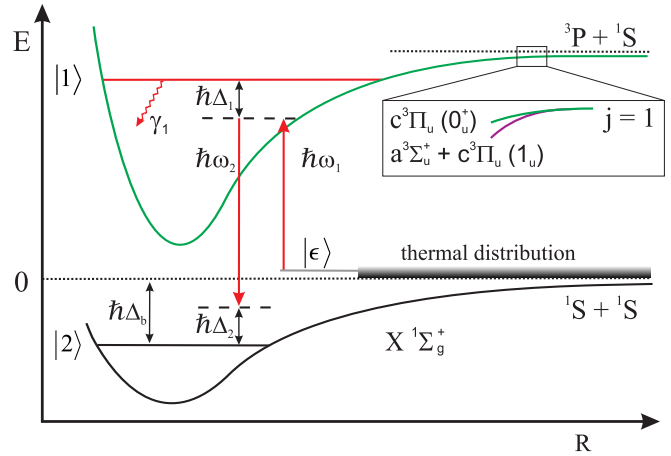


FIG. 1: Schematic overview of the two-color PA process featuring the involved molecular potentials of Ca_2 , using intermediate states near the ${}^1S_0 + {}^3P_1$ asymptote ($\lambda = 657 \text{ nm}$).

The observed levels with binding energies between 1.6 MHz and 8.2 GHz with respect to the ${}^1S_0 + {}^1S_0$ asymptote can be used to precisely determine the long range behavior of the interaction potential and to extract the s-wave scattering length a that plays a key role for the elastic scattering properties of ${}^{40}\text{Ca}$ at ultralow temperatures [15]. In a complementary measurement we have determined the molecular dipole matrix element for one transition between vibrational states in the electronically excited and the ground state potential from the Autler-Townes splitting created by coupling of these states with a resonant laser field.

II. EXPERIMENTAL SETUP

Samples of bosonic ^{40}Ca atoms are prepared at ultralow temperatures by two subsequent stages of magneto-optical traps (MOT) using the broad singlet $^1S_0 - ^1P_1$ and the strongly forbidden intercombination $^1S_0 - ^3P_1$ transitions [16]. During the cooling phases the atoms at a temperature of $10 \mu\text{K}$ are accumulating in a crossed dipole trap [15]. Following the MOT phases the temperature of the atoms in the dipole trap is further reduced by forced evaporative cooling, ramping down the dipole trap depth. About 2×10^5 atoms remain at a final temperature of $T \approx 1 \mu\text{K}$ and a maximum density of $\rho \approx 10^{19} \text{ m}^{-3}$ in the crossing region of the dipole trap beams for the experiments described here. Two PA lasers precisely tunable in the range of up to -1.4 GHz and -40 GHz relative to the atomic resonance irradiate the atomic cloud. Both lasers have a narrow linewidth $\Delta\nu \sim 1 \text{ Hz}$ realized by an offset phase-lock to an extended cavity diode laser, which is stabilized by the Pound-Drever-Hall method [17] to a high-finesse ULE cavity [18]. Thus, the difference frequency between the PA lasers inherits the narrow linewidth, enabling ultra-high resolution two-color PA spectroscopy.

The output power of both PA lasers is amplified by a system of injection-locked slave lasers. The spectral purity of the difference frequency between both PA lasers was determined from an independent beat of both lasers, which indicates about 90 % power in a sub-Hertz linewidth coherent peak. The remaining power is contained in the servo peaks of the phase lock within a bandwidth of 250 kHz. Both PA light sources are coupled to the same single-mode optical fiber to ensure that they irradiate the atomic cloud with a power of up to 20 mW from the same direction, suppressing Doppler-broadening in the recorded spectra. Both beams are linearly polarized parallel with respect to an applied magnetic field of $B = 285 \mu\text{T}$ and focused to $1/e^2$ beam waist radii $\omega_0 = 50 \mu\text{m}$ at the location of the atom cloud. We are using PA irradiation times of up to 200 ms and maximum intensities of $I_1 = 250 \text{ W cm}^{-2}$ and $I_2 = 100 \text{ W cm}^{-2}$ for the lasers driving the free-bound and the bound-bound molecular transition, respectively. Depending on the measurement configuration one of the PA lasers is scanned and the induced loss of atoms from the dipole trap is determined from absorption images using the $^1S_0 - ^1P_1$ singlet transition.

III. SIGNAL MODELING

Theoretical lineshape

The PA-spectra are evaluated using the theoretical model developed by Bohn and Julienne [12, 13]. It considers a pair of colliding atoms with a kinetic energy ϵ of the relative motion in the presence of two light fields with frequency ω_1 and ω_2 , respectively (see Fig. 1). In

the following all frequencies are expressed in angular frequencies if not noted otherwise.

The light field with frequency ω_1 is tuned closely to a molecular transition frequency which couples an excited rovibrational state $|1\rangle$ to the scattering state $|\epsilon\rangle$. The detuning from this intermediate state is Δ_1 , i.e. for $\Delta_1 = 0$ the light field is in resonance with the free-bound transition for $\epsilon = 0$ (see Fig. 1).

The second laser frequency ω_2 drives the bound-bound transition between states $|1\rangle$ and $|2\rangle$. The two color-detuning with respect to the ground state bound level located $\hbar\Delta_b < 0$ below the ground state asymptote is given by $\Delta_2 = \Delta_b - (\omega_1 - \omega_2)$. The two-color resonance at $\epsilon = 0$ corresponds to $\Delta_2 = 0$.

Generally the lifetime of the bound state $|2\rangle$ is much longer than the one of the intermediate state. Thus on the two-color resonance, the main loss mechanism proceeds through excitation to the intermediate state $|1\rangle$, from where the photoassociated molecules decay spontaneously and produce atoms with high enough energy to escape from the dipole trap.

For samples at μK temperatures only s-wave scattering is relevant, and the probability for a two-color PA loss from the input scattering channel $|\epsilon\rangle$ to the excited state $|1\rangle$ is given by the squared scattering matrix element $|S_{\epsilon 1}|^2$ [13] [36]:

$$|S_{\epsilon 1}|^2 = \frac{\gamma_1 \Gamma_{\text{stim}} \Delta_2'^2}{(\Delta_1' \Delta_2' - \Omega_{12}^2/4)^2 + ((\gamma_1 + \Gamma_{\text{stim}}) \Delta_2'/2)^2} \quad (1)$$

with $\Delta_2' = \Delta_2 - \epsilon/\hbar$ and $\Delta_1' = \Delta_1 - \epsilon/\hbar + \delta_1$. Here γ_1 denotes the decay rate of the upper molecular state, for all possible decay channels, $\hbar\delta_1$ corresponds to the light shift of the molecular level $|1\rangle$ induced by laser 1. The coupling by the laser fields is described as time-dependent interaction $-\mathbf{d}(R) \cdot \mathbf{E}_i(t) = V_{\text{opt}}^{(i)} \cos(\omega_i t)$, where the constant optical potential $V_{\text{opt}}^{(i)}$ denotes the amplitude of the harmonic perturbation, $\mathbf{d}(R)$ the molecular transition dipole operator, and $\mathbf{E}_i(t) = E_i \cos(\omega_i t)$ the electric field of laser (i) with amplitude $E_i = \sqrt{2I_i/\epsilon_0 c}$. Hence we obtain the molecular Rabi frequency

$$\Omega_{12} = \frac{1}{\hbar} \left\langle 1 \left| V_{\text{opt}}^{(2)} \right| 2 \right\rangle \quad (2)$$

for a transition between states $|1\rangle$ and $|2\rangle$, which will be explained in greater detail in Sec. VI. The free-bound excitation by laser 1 from the energy-normalized continuum state $|\epsilon\rangle$ to state $|1\rangle$ according to Fermi's golden rule the harmonic perturbation induces a stimulated rate [19]:

$$\Gamma_{\text{stim}} = \frac{\pi}{2\hbar} \left| \left\langle 1 \left| V_{\text{opt}}^{(1)} \right| \epsilon \right\rangle \right|^2. \quad (3)$$

Under the assumption that $\mathbf{d}(R)$ is only weakly depending on the internuclear separation R at long range, the total radiative decay rate of the atom pair considered

here is twice the atomic decay rate γ_{atom} , and the stimulated rate can be expressed as [20]:

$$\Gamma_{\text{stim}} = \gamma_{\text{atom}} \frac{3I_1 c^2 \pi^2}{\omega^3} f_{\text{ROT}} f_{\text{FCD}}, \quad (4)$$

where f_{ROT} contains the factor of 2 between atom pair and atomic decay rate, the polarisation dependence and the Hönl-London factor. $f_{\text{FCD}} = |\langle 1|\epsilon \rangle_{\text{rad}}|^2$ is the Franck-Condon density between the energy-normalized scattering state $|\epsilon\rangle$ and the bound state $|1\rangle$, where the subscript indicates that only the radial component is taken into account. ω is the atomic transition frequency and I_1 the laser intensity. At low energy ϵ the Wigner threshold law applies, which allows to express Γ_{stim} as:

$$\Gamma_{\text{stim}} = 2k l_{\text{opt}} \gamma_1 \quad (5)$$

with an energy-independent optical length $l_{\text{opt}}(I_1)$, the scattering wavenumber $k = (2\mu\epsilon)^{1/2}/\hbar$, and the reduced mass μ of the calcium dimer. The inelastic loss coefficient K for a thermal sample at temperature T is the thermal average

$$K = \frac{1}{h Q_T} \int_0^\infty e^{-\epsilon/k_B T} |S_{\epsilon 1}|^2 d\epsilon, \quad (6)$$

where $Q_T = (2\pi\mu k_B T/h^2)^{3/2}$ denotes the partition function for free particles. The total loss of atoms, assuming that all molecules photoassociated to state $|1\rangle$ will decay to unbound atom pairs with enough energy to leave the dipole trap, can be described by the differential equation:

$$\dot{\rho} = -\alpha\rho - 2K\rho^2, \quad (7)$$

where ρ denotes the local density of atoms inside the trap, α the loss coefficient from collisions with background gas and K the loss coefficient for PA-induced losses. In our experiment only short irradiation times τ compared to the unperturbed trap lifetime α^{-1} were used, thus inelastic scattering with background gas can be neglected i.e. $\alpha \approx 0$. In this case, the differential equation Eq. 7 can be integrated across the trapping volume to give the atom number $N(t)$ assuming that the initial thermal Gaussian distribution remains Gaussian throughout the PA process. The differential equation for the total number of atoms can then be solved:

$$N(\tau) = \frac{N_0}{1 + 2\tau N_0 K / V_{\text{eff}}}, \quad (8)$$

with an effective trap volume

$$V_{\text{eff}} = \frac{\omega_x \omega_y \omega_z}{\sqrt{8}} (m_{\text{Ca}} / (4\pi k_B T))^{3/2}$$

and trap frequencies ω_i ($i = x, y, z$). In the so-called Raman configuration for two-color PA the laser driving the free-bound transition is far detuned from the intermediate molecular level i.e. $\Delta_1 \gg (\gamma_1, \Gamma_{\text{stim}}, \Omega_{12})$. Under these conditions a maximum of the matrix element

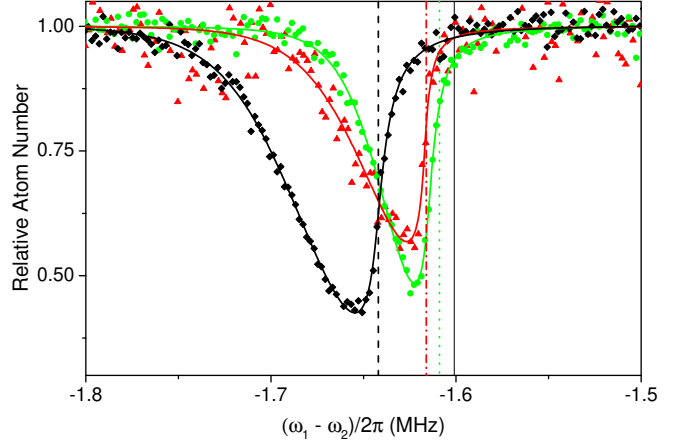


FIG. 2: Atom loss from the crossed dipole trap due to two-color PA spectroscopy as a function of the difference of the two laser frequencies for the most weakly bound molecular state in the ground state potential $X^1\Sigma_g^+$ $v_2 = 40$; $J_2 = 0$ using $v_1 = -1$; $J_1 = 1$ in $c(0_u^+)$ as the intermediate level. Spectra for three different PA-intensities are shown together with their respective fit curves and their derived resonance position indicated by vertical lines. The green dots and the vertical dotted line correspond to $I_1 = 45 \text{ W cm}^{-2}$ and $I_2 = 18 \text{ W cm}^{-2}$, black diamonds and the vertical dashed line to $I_1 = 118 \text{ W cm}^{-2}$ and $I_2 = 18 \text{ W cm}^{-2}$, red triangles and the dashed-dotted line to $I_1 = 45 \text{ W cm}^{-2}$ and $I_2 = 14 \text{ W cm}^{-2}$. The solid line at -1.601 MHz indicates the unperturbed binding energy.

$|S_{\epsilon 1}|^2$ is located at $\Delta'_2 = \frac{\Omega_{12}^2}{\Delta'_1}$. Expressing Eq. 1 in terms of the detuning from this maximum, i.e. $\Delta''_2 = \Delta'_2 - \frac{\Omega_{12}^2}{\Delta'_1}$, and assuming to stay in the vicinity of the maximum far away from the minimum at $\Delta'_2 = 0$ ($|\Delta''_2| \ll |\frac{\Omega_{12}^2}{\Delta'_1}|$), the individual lineshape for a fixed collision energy can be approximated by a Lorentzian:

$$|S_{\epsilon 1}(\Delta_2)|^2 \approx \frac{A}{(\Delta_2 - \epsilon/\hbar + \delta_{\text{shift}})^2 + (\Gamma_L/2)^2} \quad (9)$$

with parameters A , δ_{shift} , Γ_L which are related to the experimental parameters:

$$\Gamma_L = \frac{\Omega_{12}^2 (\Gamma_{\text{stim}} + \gamma_1)}{4(\Delta_1 - \epsilon/\hbar + \delta_1)^2}, \quad (10)$$

$$\delta_{\text{shift}} = \frac{\Omega_{12}^2}{4(\Delta_1 - \epsilon/\hbar + \delta_1)}, \quad (11)$$

$$A = \frac{\Gamma_{\text{stim}} \gamma_1 \Omega_{12}^4}{16(\Delta_1 - \epsilon/\hbar + \delta_1)^4}. \quad (12)$$

In Raman configuration used in our setup the deviation between the approximation and the true individual line shape is only marginal and thus can be neglected when performing the thermal averaging over collision energies ϵ . When applying Eqs. 10, 11, 12 we neglect the kinetic energy ϵ in the denominator, because its contribution is small compared to $\Delta_1 + \delta_1$. This approximation allows an

efficient modeling of the thermally broadened measured spectra (see Fig. 2) as applied in section IV. Similar to one-color PA [21], the fit approximates the integral of the thermal average (Eq. 6) by a sum of lines evenly spaced by $\delta\epsilon \approx \hbar\Gamma_L/3$

$$K \approx \sum_{n=0}^N e^{-n\cdot\delta\epsilon/k_B T} |S_{\epsilon 1}|^2 \delta\epsilon. \quad (13)$$

The number N of summation intervals has to be large enough to cover the entire line profile and is mostly depending on the temperature of the sample.

IV. MEASUREMENTS RESULTS

Ground state binding energies

We have observed two-color PA spectra of four weakly bound molecular states $|2\rangle$ in the potential $X^1\Sigma_g^+$ via intermediate bound states $|1\rangle$ of the two excited states denoted $a^3\Sigma_u^+$ and $c^3\Pi_u$ in Hund's coupling case (a). Near the $^3P_1 + ^1S_0$ asymptote the spin-orbit interaction becomes dominant and the adiabatic potentials are more accurately described by Hund's case (c) potentials $c0_u^+$ and $(a, c)1_u$ being a strong mixture of the two case (a) states (Fig. 1). In the experiment we have used $v_1 = -1, J_1 = 1, \Omega = 1$ and $v_1 = -1, J_1 = 1, \Omega = 0$ [22] as intermediate states from which laser 1 was detuned by $\Delta_1/2\pi \approx \pm 1$ MHz. Here J denotes the total angular momentum of the respective state. The PA lines were then fitted using the procedure described before to assess the resonance frequency at zero-collision energy i.e. $\epsilon = 0$.

Three spectra of the most weakly bound state $v_2 = 40; J_2 = 0$ in $X^1\Sigma^+$ for different experimental parameters and their respective fitted lineshapes are shown in Fig. 2. Their characteristics shall be discussed in the following. The level $v_1 = -1; \Omega = 0$ has been used as the intermediate level in the Raman configuration PA with the large detuning $\Delta_1/2\pi \approx +1$ MHz. All spectra were taken at a temperature of $T = 1.15 \mu\text{K}$ determined from time of flight measurements. They all show the typical asymmetric thermal broadening that is a characteristic feature of photoassociation spectra when the mean kinetic energy is large compared to the width of the excited level. If we used the energy dependence of Γ_L in Eq. 10 through Γ_{stim} according to Eq. 5 and assumed $\gamma_1 = 2\gamma_{\text{atom}}$ during the fitting procedure we obtained nonphysical values for the set of parameters $\{T, \Omega_{12}, l_{\text{opt}}\}$. This behavior points towards a larger effective decay rate γ_1 . A similar effect of enlarged molecular decay rates has been reported for PA spectra of ^{88}Sr [23]. To compensate for this we use an energy-independent effective linewidth Γ_L for a given experimental condition defined by the intensities of laser 1 and 2, detuning Δ_1 and temperature T . For the fit of the profiles according to Eq. 13 we represent the squared matrix

element $|S_{\epsilon 1}|^2$:

$$\frac{|S_{\epsilon 1}(\omega_1 - \omega_2)|^2}{\frac{A^{\text{eff}}\sqrt{\epsilon}}{(-\omega_1 - \omega_2) - \epsilon/\hbar - \Delta_b^{\text{eff}})^2 + (\Gamma_L/2)^2}} \approx \quad (14)$$

with effective fit parameters Δ_b^{eff} that contains light shifts induced by the spectroscopy and trapping lasers (compare Figs. 3, 4, 5) and $A^{\text{eff}} = A/\sqrt{\epsilon}$ to account for the energy dependence of the stimulated rate in A . Increasing the free-bound intensity I_1 from the green (circles) to the black (diamonds) curves in Fig. 2 leads to a considerable light shift of the resonance position. The linewidth Γ_L increases from 6.0 kHz to 9.2 kHz while the temperature derived by the fit remains nearly constant about 20 % below the value determined from the time of flight measurement. This behavior is connected to the change in the stimulated rate in Eq. 4 or Eq. 5 and to an increased light shift δ_1 , leading to a broader individual linewidth.

In the same way a decrease of bound-bound laser intensity between the green (dots) and red (triangles) data points leads to a decrease of Γ_L from 6.0 kHz to 4.3 kHz. This is consistent with a reduced molecular Rabi frequency Ω_{12} that also shifts the resonance position according to Eq. 11. The fit correctly reproduces the theoretical expectations regarding individual PA linewidth and PA rates as a function of increasing PA intensities I_1, I_2 . The sample temperature determined by the fit is slightly underestimated.

Experimental noise near the steep edge in the spectra can have enormous impact on some of the fit parameters. Fortunately, the resonance position determined by the fit is very robust against changes in $\Gamma_L, \Delta_b^{\text{eff}}, A^{\text{eff}}, T$ and is mostly determined by the steep edge, that is only a few kHz wide (see Fig. 2). Thus the zero-energy resonance position of the molecular level can be determined with high reliability.

In addition to the thermal shift, the observed line is also shifted due to the ac Stark effects from the two PA lasers and from the trapping laser and should be contained in the parameter Δ_b^{eff} . These shifts were determined independently by extrapolation to zero laser intensity from a series of measurements for different intensities as shown in Figs. 3, 4, 5 to reduce the model dependence from the representation of $|S_{\epsilon 1}|^2$ and to take into account the effect by the trapping laser when deriving the desired binding energies from resonance positions. An overview of all considered corrections on the final resonance position and their respective uncertainties is given in Tab. I. An additional uncertainty contribution of the ac Stark shift by laser 2 arises according to Eq. 11 by the detuning of the intermediate level. Multiple measurements with detuning $\Delta_1/2\pi$ in the range $\pm(400 - 1000)$ kHz indicate an uncertainty of 1 kHz for the resonance position.

As mentioned above, the fit routine underestimates the temperature of the atomic sample by about 20 % compared to the temperature from time-of-flight measurements. We account for this deviation by an uncertainty

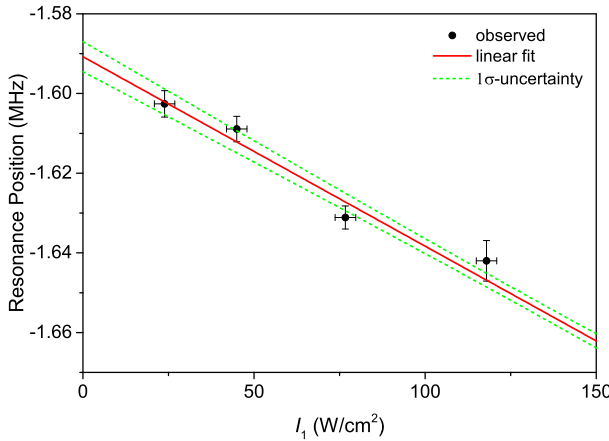


FIG. 3: Measured resonance position of $v = 40$, $J = 0$ depending on the free-bound PA laser intensity I_1 . The solid red line shows a linear extrapolation to zero intensity while the green dotted lines give the 1σ -uncertainty interval. Measurements were taken at $I_2 = 18.3 \text{ Wcm}^{-2}$, $I_{\text{DT}} = 44.2 \text{ Wcm}^{-2}$

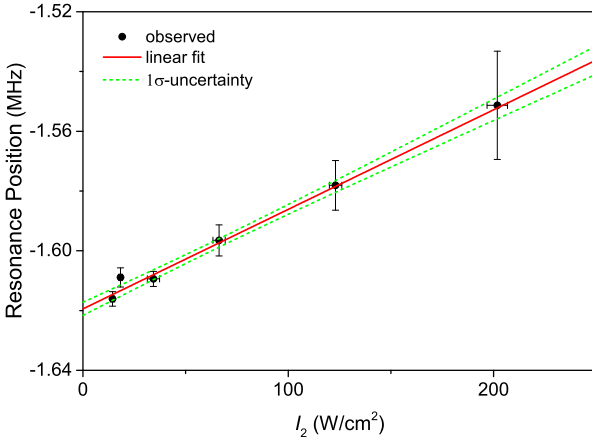


FIG. 4: Measured resonance position of $v = 40$, $J = 0$ depending on the bound-bound PA laser intensity I_2 . The solid red line shows a linear extrapolation to zero intensity while the green dotted lines give the 1σ -uncertainty interval. Measurements were taken at $I_1 = 45.0 \text{ Wcm}^{-2}$, $I_{\text{DT}} = 44.2 \text{ Wcm}^{-2}$

of the derived binding energy of $0.1 \cdot \epsilon/\hbar \approx 2 \text{ kHz}$ (see Tab. I).

We estimate the combined uncertainty of the aforementioned sources combined with other sources of technical nature to be 3 kHz. Among these are small nonlinearities of the atom number estimation from the absorption imaging, variations of dipole trap power and the ramp procedure for the evaporation cooling, residual contributions of unwanted frequencies stemming from the offset-locking of the spectroscopy lasers and residual magnetic fields.

The unperturbed binding energies $\hbar\Delta_b^{\text{exp}}$ including all corrections and uncertainties are shown in Tab. I.

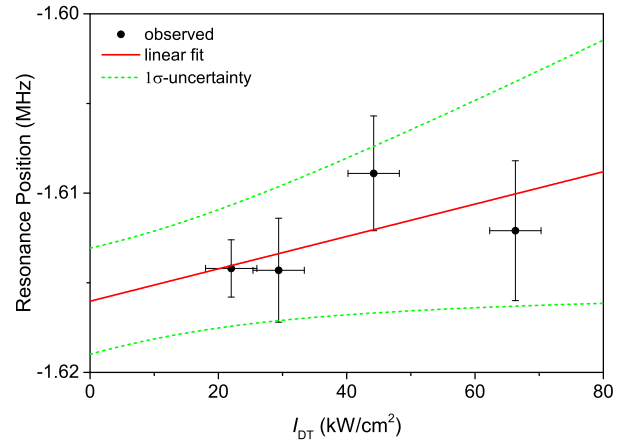


FIG. 5: Measured resonance position of $v = 40$, $J = 0$ depending on the dipole trap laser intensity I_{DT} . The solid red line shows a linear extrapolation to zero intensity while the green dotted lines give the 1σ -uncertainty interval. Measurements were taken at $I_1 = 45.0 \text{ Wcm}^{-2}$, $I_2 = 18.3 \text{ Wcm}^{-2}$

V. MOLECULAR POTENTIALS

Molecular potentials are needed for the prediction of binding energies, calculating Franck-Condon densities (FCD) in Eq. 4, and modeling bound-bound transitions with appropriate Franck-Condon factors (FCF).

The excited state potentials at the asymptote $^3P_1 + ^1S_0$ were determined in [22] and the vibrational levels are represented by a multi-component wave function, which we will describe most conveniently for the calculation of the electric dipole transition by the Hund's case (e) basis $|^1S_0 + ^3P_j, l, J\rangle$. The first part of the basis vector describes the relevant atom pair asymptote with the total atomic angular momentum j , l the angular momentum of the pair rotation and J the total angular momentum. Because the starting level in the present experiment is always the s-wave continuum, corresponding to $J = 0$ and parity +, we have only to consider the excited levels $J = 1$, parity -, thus only the three possible basis states

$$|^1S_0 + ^3P_1, 0, 1\rangle, \quad (15)$$

$$|^1S_0 + ^3P_1, 2, 1\rangle, \quad (16)$$

$$\text{and } |^1S_0 + ^3P_2, 2, 1\rangle. \quad (17)$$

Because of the electric dipole selection rule $\Delta l = 0$ from these basis states only the component $|^1S_0 + ^3P_1, 0, 1\rangle$ is needed for the calculation of the Franck-Condon densities with the continuum $|^1S_0 + ^1S_0, 0, 0\rangle$ and the two first components for the Franck-Condon factors with the bound levels $|^1S_0 + ^1S_0, 0, 0\rangle$ or $|^1S_0 + ^1S_0, 2, 2\rangle$.

The molecular ground state potential $X^1\Sigma_g^+$ is based on spectroscopic measurements by [14] for the short range part and on the new data for the long range branch as

bound level	$v = 38 J = 2$	$v = 39 J = 0$		$v = 39 J = 2$			$v = 40 J = 0$
intermediate state detuning $\Delta_1/(2\pi)$	$v_1 = -1\Omega = 0$ -1 101(10)	$v_1 = -1\Omega = 1$ -1 001(10)	1 016(10)	-1 001(10)	-924(10)	+900(10)	$v_1 = -1\Omega = 0$ +978(10)
ac Stark free-bound laser	1(2)	0(10)	-1(6)	0(3)	0(5)	-24(24)	22(4)
ac Stark bound-bound laser	4(2)	30(5)	-9(5)	9(3)	8(3)	-10(2)	-6(2)
ac Stark dipole trap	1(3)	-17(17)	-4(4)	0(4)	0(3)	0(3)	-3(3)
extrapolated position	-8 218 897(4)	-1 387 457(20)	-1 387 439(9)	-1 005 369(6)	-1 005 361(7)	-1 005 379(24)	-1 601(6)
weighted average	-8 218 897(4)	-1 387 442(8)		-1 005 366(5)			-1 601(6)
systematic uncertainty	0(3)	0(3)		0(3)			0(3)
unperturbed energy $\Delta_b^{\text{exp}}/(2\pi)$	-8 218 894(5)	-1 387 444(9)		-1 005 367(6)			-1 601(7)
calc. energy $\Delta_{\text{calc}}/(2\pi)$	-8 218 896	-1 387 437		-1 005 372			-1 599

TABLE I: The binding energies $\hbar\Delta_b^{\text{exp}}$ with corrections and corresponding uncertainties. All values are given in kHz.

described by the conventional power expansion in $1/R$

$$V_X = -f_6(R) \frac{C_6}{R^6} - \frac{C_8}{R^8} - \frac{C_{10}}{R^{10}}. \quad (18)$$

By the function $f_6(R)$ we apply the retardation correction as calculated by Moszynski *et al.* [24], which turned out to be essential for describing the asymptotic levels within their experimental uncertainty. This correction is only significant to the first term in the equation due to the very long range nature of the van der Waals interaction. An additional exchange term is regularly used in the mathematical representation of the long range potential. Such term is not needed for the description in our case, due to the van der Waals term being large compared to a possible exchange energy in the range $R > 1.1$ nm in which Eq. 18 is applied.

ref.	C_6	C_8	C_{10}
	$10^7 \text{ cm}^{-1} \text{\AA}^6$	$10^8 \text{ cm}^{-1} \text{\AA}^8$	$10^9 \text{ cm}^{-1} \text{\AA}^{10}$
[14]	1.0023	3.808	5.06
[25]	1.003		
[26]	1.022	3.010	8.057
[27]	1.055	3.060	8.344
this work	1.0348	2.997	10.88

TABLE II: Comparison of long range parameters at the asymptote $^1S_0 + ^1S_0$ derived in this work with experimental results from Allard *et al.* [14] and theoretical results from Ciurylo *et al.* [25], Porsev *et al.* [26] and Mitroy and Zhang [27]

In a least squares fit of all known data for the ground state (in total 3586 data points) the long range parameters were varied including as additional condition the theoretical coefficients C_i for $i = 6, 8, 10$ [25–27, 29] applying their estimated uncertainties from the calculation as weights in the fit. The fit reveals in total a normalized standard deviation $\sigma = 0.76$, a good fit should result to values close to one, if the applied uncertainties are well justified and the theoretical model is appropriate.

Method	a/a_0
molecular spectroscopy [14]	200 - 800
$^1S_0 + ^1P_1$ photoassociation [28]	340 - 700
BEC mean field [15]	≈ 440
this work	308.5 (50)

TABLE III: $^1S_0 + ^1S_0$ scattering length a of ^{40}Ca in comparison with experimental results, $a_0 \approx 53$ pm denotes the Bohr radius

Thus we obtain a very satisfactory result. In detail, the spectroscopic data from [14] are represented within their respective experimental uncertainty, and the binding energies of the asymptotic levels in the last line of Tab. I are within their assumed uncertainties, only level $v = 39, J = 2$ touches the upper edge. The derived long range parameters are shown in Tab. II and are compared with earlier results from experiment and theory. With this improved potential representation the uncertainty of the calculated scattering length $a = 308.5(50)a_0$ decreases by more than a factor of 10 compared to former results (Tab. III) The remaining uncertainty originates to a significant part from the correlation between the long range parameters C_6, C_8, C_{10} . A much denser set of eigenvalues at the ground state asymptote would be required to break this correlation. Because the last bound state is very close to the asymptote, namely -1.6 MHz, one could try to estimate the scattering length a from a simple relation between binding energy and scattering length [30]

$$a = \bar{a} + \frac{\hbar}{\sqrt{2\mu E_b}}, \quad (19)$$

where \bar{a} is the background scattering length, μ the molecular reduced mass and E_b the binding energy. \bar{a} depends on the long range form of the potential, namely C_6 and if the value \bar{a} is small compared to the expected scattering length, i.e. the binding energy is sufficiently small, the scattering length can be directly determined by the binding energy with good approximation. Using the C_6

value from Tab. III one calculates $\bar{a} = 53.4 a_0$, which does not justify to only apply the second part of Eq. 19. The full equation results to $a = 291 a_0$ and comes close to the value obtained from the full potential. The difference indicates that the higher order terms in the long range function cannot be neglected.

From mass scaling we also calculate the scattering length of other natural isotopes of calcium as shown in Tab. IV using the full potential of $X^1\Sigma_g^+$. Scattering

Isotope	a/a_0
^{40}Ca	308.5(50)
^{42}Ca	297 (6)
^{43}Ca	43.7 (10)
^{44}Ca	399 (7)
^{46}Ca	1970 (20)
^{48}Ca	-281 (10)

TABLE IV: Scattering length a of homonuclear pairs for different natural isotopes of calcium, $a_0 \approx 53$ pm Bohr radius

lengths for other isotopes of Ca are reported [31, 32] using earlier experimental results on ^{40}Ca from our group [14, 15], thus these values suffer from the lower precision of those data.

The newly determined potential was applied to calculate the desired FCD and FCF (see Tab. V) for evaluation of the spectroscopic observations as detailed in section III and the following paragraph.

VI. AUTLER-TOWNES SPECTRA AND MOLECULAR DIPOLE MATRIX ELEMENT

We have also used a different configuration of PA laser detunings, where the bound-bound laser was tuned to resonance, i.e. $\Delta_2 - \Delta_1 \approx 0$, and instead the free-bound laser was scanned across the excited state resonance. Through coupling of the two bound states by the resonant light field dressed states are created that lead to two resonances: the Autler-Townes doublet [33]. The two resonances are separated by the molecular Rabi frequency Ω_{12} :

$$\Omega_{12} = \sqrt{f_{\text{ROT}}} \sqrt{f_{\text{FCF}}} \sqrt{\gamma_{\text{atom}}} \sqrt{I_2 \frac{6c^2\pi}{\omega^3\hbar}}. \quad (20)$$

Here f_{ROT} is the rotational factor related to the coupling of $J_1, M_1 - J_2, M_2$ and the ratio of atomic and molecular decay rate. The Franck-Condon factor $f_{\text{FCF}} = |\langle 1|2 \rangle_{\text{rad}}|^2$ giving a measure for the strength of molecular transitions is related to the overlap integral of the wave functions of the bound states using the selection rule for electric dipole transitions to choose the proper component of the multi-component wavefunctions. In this case $|1\rangle = |^1S_0 + ^3P_1, 0, 1\rangle$ and $|2\rangle = |^1S_0 + ^1S_0, 0, 0\rangle$ for the coupling $J = 1 - 0$ and $|1\rangle = |^1S_0 + ^3P_1, 2, 1\rangle$ and $|2\rangle = |^1S_0 + ^1S_0, 2, 2\rangle$ for the coupling $J = 1 - 2$. The

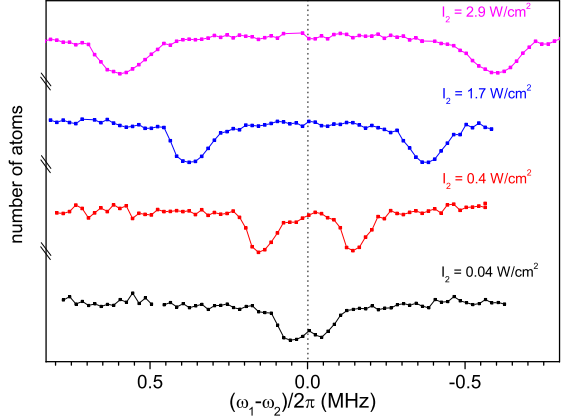


FIG. 6: Atomic loss spectra when scanning the free-bound PA laser across the $v_1 = -1$, $\Omega = 1$ molecular resonance in Autler-Townes configuration. The bound-bound laser was set to be resonant between $v_2 = 39$, $J_2 = 0$ and the before mentioned excited state. Autler-Townes splitting for different bound-bound PA laser intensity I_2 .

factor f_{ROT} is calculated in the Hund's case (e) basis. With conventional angular momentum algebra [34] for a transition $|j_1, l_1, J_1, M_1\rangle$ to $|j_2, l_2, J_2, M_2\rangle$ applying the decoupling of $l_{1,2}$ because the electric dipole operator does not act in the rotational space we obtain the rotational factor:

$$f_{\text{ROT}} = (2J_1 + 1)(2J_2 + 1)w6j(j_1, J_1, l_1, J_2, j_2, 1)^2 \delta(l_1, l_2) w3j(J_1, 1, J_2, -M_1, q, M_2)^2 \cdot 2 \cdot (2j_1 + 1), \quad (21)$$

where $w3j$ and $w6j$ are the conventional Wigner-nj symbols and $q = 0, \pm 1$ indicates the polarization of the light field. For the present two cases with π polarized light and $M_1 = M_2 = 0$ the values are 2 and $4/5$, respectively.

We have measured the splitting of the Autler-Townes doublet for different intensities I_2 to validate the approximation that the atomic dipole moment governs the molecular transition between these long range levels. The recorded spectra are shown in Fig. 6. The resonance curves show two features of almost identical amplitude indicating that the second PA-laser was indeed tuned closely to the bound-bound transition, i.e. the detuning was $\Delta_1 - \Delta_2 \approx 0$ [13].

From the measured splitting we determined the Rabi frequencies for different PA laser intensities, which are plotted as a function of laser intensity I_2 in Fig. 7. They are consistent with the expected square-root behavior (red solid line). From the experimental values we determined the Franck-Condon factor for a transition from the level $v_1 = -1$, $J_1 = 1$ of the excited state state (ac) $\Omega = 1$ to the level $v_2 = 39$, $J = 0$. A fit of Eq. 20 to the data yields $f_{\text{FCF,exp}} = 0.45(9)$, which is in fair agreement to the theoretical prediction $f_{\text{FCF,theo}} = 0.54$ (see Tab. V). The dashed line in Fig. 7 shows the theoretical

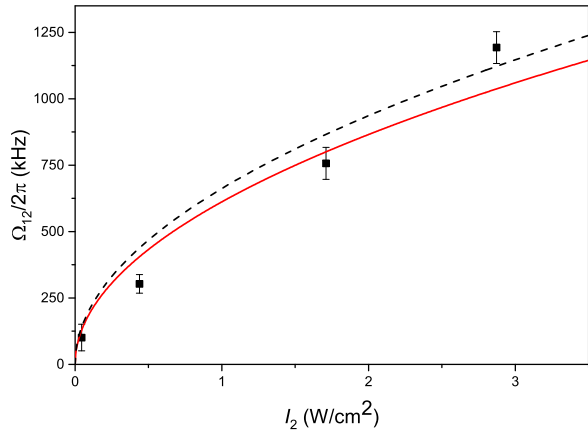


FIG. 7: Measured molecular Rabi frequencies Ω_{12} from Autler-Townes spectra (dots) of the $v_1 = -1$, $\Omega = 1$ molecular resonance in dependence of the bound-bound laser intensity I_2 . The black dashed line indicates theoretical prediction following Eq. 20 with $f_{\text{FCF, theo}} = 0.54$ determined from molecular potentials while the red solid line is a fit to the data.

expectation. The small deviation could be explained by an additional uncertainty of the absolute intensity of the bound-bound PA laser at the position of the ultracold atoms due to uncertainty from the beam waist measurement and the alignment of dipole trap and focus of the PA-beam or alternatively the assumed molecular transition dipole moment deviates slightly from being $\sqrt{2}$ times the atomic dipole moment.

The molecular potentials determined from the ground state binding energies measured in Raman configuration PA and the excited state potentials [22] can be used for calculating $f_{\text{FCF, theo}}$ for arbitrary transitions between states close to the excited state asymptote $^3P_1 + ^1S_0$ and rovibrational states in $X^1\Sigma_g^+$. Tab. V shows a set of calculated values of f_{FCF} for those excited states with an appreciable Franck-Condon density f_{FCD} between the ground state continuum and the respective excited state, which would be desirable for easy PA spectroscopy. When calculating transition rates using the values given in Tab. V one also has to consider the additional f_{ROT} for transitions to final states with $J_2 = 0, 2$, respectively. For calculating molecular radiation decay rates we have to sum over the polarization q , i.e. $\gamma_{1 \rightarrow 2} = \gamma_{\text{atom}} f_{\text{FCF}} \Sigma_q f_{\text{ROT}}$, which for the present case with atomic angular momenta 1 and 0 results in the value 2 independent of the molecular angular momentum. We obtain with values from Tab. V for the measured transition a spontaneous decay rate from the state $v_1 = -1$, $\Omega = 1$, $J_1 = 1$ to $v_2 = 39$, $J_2 = 0$ of $\gamma_{1 \rightarrow 2} = 1.08 \cdot \gamma_{\text{atom}}$ and to $v_2 = 39$, $J_2 = 2$ of $\gamma_{1 \rightarrow 2} = 0.30 \cdot \gamma_{\text{atom}}$. Tab. V gives also in the last line the remaining continuum contribution. The sum of all Franck-Condon factors of a single excited state differs slightly from one, because it only represents the part for electric dipole transitions while the spin-orbit mixing for

	Ω	0	1	0	1	0	1
J_2	$v_2 \setminus v_1$	-1	-1	-2	-2	-3	-3
0	40	0.02	$< 10^{-2}$	$< 10^{-3}$	$< 10^{-2}$	$< 10^{-3}$	$< 10^{-3}$
2	39	0.38	0.15	0.25	0.04	0.03	0.02
0	39	0.06	0.54	0.12	0.15	0.01	0.04
2	38	$< 10^{-2}$	$< 10^{-4}$	0.23	0.12	0.40	0.13
0	38	$< 10^{-2}$	$< 10^{-2}$	0.07	0.29	0.17	0.33
2	37	$< 10^{-3}$	$< 10^{-6}$	$< 10^{-2}$	$< 10^{-3}$	0.13	0.06
0	37	$< 10^{-3}$	$< 10^{-3}$	$< 10^{-2}$	$< 10^{-2}$	0.05	0.13
cont.		0.53	0.30	0.31	0.39	0.17	0.27

TABLE V: Calculated Franck-Condon factors f_{FCF} for transitions from bound levels ($v_1, J_1 = 1$) of the states $\Omega = 1_u$ and 0_u^+ of the coupled system $a^3\Sigma_u^+$ and $c^3\Pi_u$ to bound levels ($v_2, J_2 = 0, 2$) of the ground state $X^1\Sigma_g^+$. The last line gives the fraction of excited molecules decaying back to continuum states near the ground state asymptote with $J = 0, 2$

the excited state results in a small component with total atomic angular momentum $j = 2$, which will not decay by electric dipole radiation to the ground state with $j = 0$.

VII. CONCLUSION

This paper shows the results of our study of the $^1S_0 - ^1S_0$ asymptote of the calcium dimer by means of two-color photoassociation in Raman and Autler-Townes configuration. The investigation of the collisional properties of ultracold thermal calcium molecules near the dissociation limit gives access to the previously experimentally not well characterized long-range part of the ground state potential $X^1\Sigma_g^+$. Including earlier measurements of deeply bound states [14], an improved description of the molecular potential near the dissociation asymptote was derived and also a highly improved value for the ^{40}Ca s-wave scattering length $a = 308.5(50) a_0$ was calculated. The scattering length for other natural isotopes of calcium were also derived using the improved description of the ground state potential.

With the help of a coupled channel calculation, transition moments between excited [22] and ground state levels have been derived and compared with experimental results from Autler-Townes measurements. The values show good agreement and confirm the validity of the theoretical description. This will allow calculations of transition paths for efficient creation of molecules in predetermined rovibrational states. According to Tab V for every asymptotic excited state only a few transitions to bound ground states show a substantial FCF allowing spontaneous decay to these states for use as a starting level in future experiments like coherent population transfer. For example about 54 % of the molecules produced in the excited state $v_1 = -1$, $J_1 = 1$ are expected to decay to the ground state $v_2 = 39$, $J_2 = 0$.

The improved understanding of the ground state al-

lows the calculation of an optical length l_{opt} for the different excited molecular states. For an incident intensity of $I_1 = 3.0 \text{ Wcm}^{-2}$ we calculate a value of about $l_{\text{opt}} = 10^3 a_0$ for the least bound state $v_1 = -1$, $\Omega = 0$, under the assumption that the molecules in this state only decay radiatively with the rate $\gamma_1 = 2\gamma_{\text{atom}}$. These results lead to a promising prospect for the implementation of low-loss optical Feshbach resonances [35] for atom species with a very narrow intercombination line like calcium, i.e. an optically induced change of the scattering length $a_{\text{opt}} \approx \pm 300 a_0$ can be achieved at a detuning of about 30 times the natural linewidth, effectively reducing the scattering length close to zero or even negative values.

Acknowledgments

We thank Max Kahmann for experimental support in the early stage of this work, Andreas Koczwara for technical support with the phase-lock of the second spectroscopy laser setup and E. Tiesinga for directing us to the reference regarding the calculation of the retardation in calcium pair interaction. This work was supported by Deutsche Forschungsgemeinschaft (DFG) through the *Center of Quantum Engineering and Space-Time Research (QUEST)* of the Leibniz Universität Hannover, through the Research Training Group 1729 *Fundamentals and Applications of Ultra Cold Matter* and CRC 1227 *Designed Quantum States of Matter*.

[1] K. M. Jones, E. Tiesinga, P. D. Lett, and P. S. Julienne, Rev. Mod. Phys. **78**, 483 (2006).

[2] C. Chin, R. Grimm, P. Julienne, and E. Tiesinga, Rev. Mod. Phys. **82**, 1225 (2010).

[3] E. R. I. Abraham, W. I. McAlexander, J. M. Gerton, R. G. Hulet, R. Côté, and A. Dalgarno, Phys. Rev. A **55**, R3299 (1997).

[4] F. A. van Abeelen and B. J. Verhaar, Phys. Rev. A **59**, 578 (1999).

[5] H. Wang, A. N. Nikolov, J. R. Ensher, P. L. Gould, E. E. Eyler, W. C. Stwalley, J. P. Burke, J. L. Bohn, C. H. Greene, E. Tiesinga, et al., Phys. Rev. A **62**, 052704 (2000).

[6] C. C. Tsai, R. S. Freeland, J. M. Vogels, H. M. J. M. Boesten, B. J. Verhaar, and D. J. Heinzen, Phys. Rev. Lett. **79**, 1245 (1997).

[7] N. Vanhaecke, C. Lisdat, B. T'Jampens, D. Comparat, A. Crubellier, and P. Pillet, Eur. Phys. J. D **28**, 351 (2004).

[8] J. Kim, U. Rapol, S. Moal, J. Léonard, M. Walhout, and M. Leduc, Eur. Phys. J. D **31**, 227 (2004).

[9] Y. N. Martinez de Escobar, P. G. Mickelson, P. Pellegrini, S. B. Nagel, A. Traverso, M. Yan, R. Côté, and T. C. Killian, Phys. Rev. A **78**, 062708 (2008).

[10] M. Kitagawa, K. Enomoto, K. Kasa, Y. Takahashi, R. Ciuryło, P. Naidon, and P. S. Julienne, Phys. Rev. A **77**, 012719 (2008).

[11] C. Degenhardt, H. Stoehr, C. Lisdat, G. Wilpers, H. Schnatz, B. Lipphardt, T. Nazarova, P.-E. Pottie, U. Sterr, J. Helmcke, et al., Phys. Rev. A **72**, 062111 (2005).

[12] J. L. Bohn and P. S. Julienne, Phys. Rev. A **54**, R4637 (1996).

[13] J. L. Bohn and P. S. Julienne, Phys. Rev. A **60**, 414 (1999).

[14] O. Allard, C. Samuelis, A. Pashov, H. Knöckel, and E. Tiemann, Eur. Phys. J. D **26**, 155 (2003).

[15] S. Kraft, F. Vogt, O. Appel, F. Riehle, and U. Sterr, Phys. Rev. Lett. **103**, 130401 (2009).

[16] C. Degenhardt, T. Nazarova, C. Lisdat, H. Stoehr, U. Sterr, and F. Riehle, IEEE Trans. Instrum. Meas. **54**, 771 (2005).

[17] R. W. P. Drever, J. L. Hall, F. V. Kowalski, J. Hough, G. M. Ford, A. J. Munley, and H. Ward, Appl. Phys. B **31**, 97 (1983).

[18] T. Nazarova, C. Lisdat, F. Riehle, and U. Sterr, J. Opt. Soc. Am. B **25**, 1632 (2008).

[19] C. Cohen-Tannoudji, J. Dupont-Roc, and G. Grynberg, *Atom-Photon Interactions* (Wiley, New York, 1992).

[20] R. Ciuryło, E. Tiesinga, and P. S. Julienne, Phys. Rev. A **74**, 022710 (2006).

[21] K. M. Jones, P. D. Lett, E. Tiesinga, and P. S. Julienne, Phys. Rev. A **61**, 012501 (1999).

[22] M. Kahmann, E. Tiemann, O. Appel, U. Sterr, and F. Riehle, Phys. Rev. A **89**, 023413 (2014).

[23] T. Zelevinsky, M. M. Boyd, A. D. Ludlow, T. Ido, J. Ye, R. Ciuryło, P. Naidon, and P. S. Julienne, Phys. Rev. Lett. **96**, 203201 (2006).

[24] R. Moszynski, G. Lach, M. Jaszunski, and B. Bussery-Honvault, Phys. Rev. A **68**, 052706 (2003).

[25] R. Ciuryło, E. Tiesinga, S. Kotochigova, and P. S. Julienne, Phys. Rev. A **70**, 062710 (2004).

[26] S. G. Porsev and A. Derevianko, J. Exp. Theor. Phys. **102**, 195 (2006).

[27] J. Mitroy and J.-Y. Zhang, J. Chem. Phys. **128**, 134305 (2008).

[28] F. Vogt, C. Grain, T. Nazarova, U. Sterr, F. Riehle, C. Lisdat, and E. Tiemann, Eur. Phys. J. D **44**, 73 (2007).

[29] S. G. Porsev and A. Derevianko, Phys. Rev. A **65**, 020701(R) (2002).

[30] G. F. Gribakin and V. V. Flambaum, Phys. Rev. A **48**, 546 (1993).

[31] U. Dammalapati, L. Willmann, and S. Knoop, Phys. Rev. A **84**, 054703 (2011).

[32] J.-C. Zhang, J.-F. Sun, Z.-L. Zhu, and Y.-F. Liu, Phys. Scr. **87**, 025302 (2013).

[33] S. H. Autler and C. H. Townes, Phys. Rev. **100**, 703 (1955).

[34] A. R. Edmonds, *Angular momentum in quantum mechanics* (Princeton University Press, Princeton, New Jersey, 1957).

[35] R. Ciuryło, E. Tiesinga, and P. S. Julienne, Phys. Rev. A **71**, 030701 (2005).

[36] Note that the Rabi frequency Ω_{12} differs from the formula given in [13]. Our definition follows the convention in

[19] representing the frequency for transferring amplitude between the two bound states.